Organogels from Double-Chained Vitamin C Amphiphilic Derivatives

ChemPubSoc Europe

DOI: 10.1002/cphc.201601267

CHEMPHYSCHEM Articles

Organogels from Double-Chained Vitamin C Amphiphilic Derivatives

Elia Tempestini,[a] Martina Bucci,[a] Vincenzo Mastromartino,[a] Marianna Gori,[a] Damiano Tanini,[a] Moira Ambrosi,[a] Emiliano Fratini,[a] Antonella Capperucci,[a] and Pierandrea Lo Nostro*[a, b]

The syntheses and physicochemical characterization of double-chained amphiphilic compounds obtained from vitamin C are reported: dialkanoyl-5,6-*O*-ascorbic acid esters (Di-ASC*n*, $n=8$, 10, and 12). The acetyl-5-dodecanoyl-6-ascorbic acid ester is synthesized and investigated for comparison. These products are quite insoluble in water and in polar solvents, although they form homogeneous dispersions in cyclohexane. Upon cooling, these dispersions turn into a gel-like phase. Differential scanning calorimetry, FTIR spectroscopy, and small- and wide-angle X-ray scattering experiments are performed to investigate the properties of pure solids and their liquid dispersions. Di-ASC*n* retain the same redox properties of the parent molecule and represent a valid candidate for the production of nanosized protective carriers for valuable guests that are sensitive to oxidative radical attack. Moreover, the contribution of the vitamin C hydroxyl group in position 5 to the overall hydration properties of single- and double-chained amphiphilic derivatives is discussed.

1. Introduction

Previously, we extensively investigated the solid-state and self-assembly properties of amphiphilic single-chained alkanoyl-6-*O*-ascorbic acid esters (ASC*n*; $8 \leq n \leq 18$),[1–8] bolaforms,[9,10] and branched derivatives.[11] In these compounds, a hydrophobic side chain is linked through an ester bond to the –OH group in position 6 of the lactone ring. The synthesis involves the reaction between a carboxylic acid and L-ascorbic acid in concentrated sulfuric acid, but the lactone ring remains untouched, with its original and strong redox activity.[12] Our first motivation in those studies was the conversion of vitamin C, which is soluble only in aqueous or very polar media, into chemical species that retained its pristine antioxidant power, but that could be dissolved in a lipophilic environment, such as an organic solvent or the inner compartment of a membrane. Moreover, the self-assembled nanostructures formed by these surfactants are among the best candidates for drug delivery of hydrophobic, easily oxidizable drugs.[13–16] Depending on the length of the lipophilic side chain, the ASC*n* surfactant behaves differently when dispersed in water: for $n \leq 10$, the amphiphile forms micelles that, upon cooling, turn into a densely packed hydrated lamellar phase, the coagel, which exhibits sharp XRD patterns and optical birefringence. Instead, for $n \geq 12$, upon heating, the coagel forms a translucent and less viscous phase that is commonly referred to as a gel. We fully investigated the micelle-to-coagel or gel-to-coagel phase transitions, and the different types of water, that is, strongly bound, intermediate, and bulk water.[17,18] The coagel phase is usually depicted of as a set of piled up surfactant lamellae separated by thin interlayers (approximately 1 nm) of strongly bound water molecules.[18–23] In the coagel state, the aliphatic chains are in the *all-trans* planar conformation and well packed in an orthorhombic crystal lattice.[21,22,24] On the other hand, in the gel state, the hydrophobic tails are arranged in a hexagonal lattice, they rotate or vibrate around the main chain axis, and the water interlayer thickness is about 100 nm.[21]

Supramolecular gels are viscoelastic materials formed by low-molecular-weight building blocks that spontaneously self-assemble into thermoreversible three-dimensional structures. Hydrogen-bonding (HB), donor–acceptor, π-stacking, and van der Waals interactions lead to the formation of fibers that can entrap significant amounts of solvent molecules inside the interstices of the 3D network.[25] Due to their structure and performances, gels find interesting applications in photography, tissue engineering, cosmetics, controlled drug delivery, template synthesis of nanoparticles and inorganic nanostructures, sensors, and food processing.[26]

The thermal stabilities of the gelators, their solubilities, and capabilities to self-assemble in water and organic solvents are remarkably affected by the nature and length of their hydrophobic segment and by their affinity for the solvent.[25–27]

Organogels are produced by hydrophobic vitamin C derivatives in organic solvents, such as cyclohexane, chloroform, *i*-octane, or dichloromethane. The addition of tiny amounts of

[a] E. Tempestini, M. Bucci, V. Mastromartino, M. Gori, Dr. D. Tanini, Dr. M. Ambrosi, Dr. E. Fratini, Dr. A. Capperucci, Prof. P. Lo Nostro
Department of Chemistry, University of Florence
Via della Lastruccia 3–13, 50019 Sesto Fiorentino (Italy)
E-mail: pierandrea.lonostro@unifi.it

[b] Prof. P. Lo Nostro
Enzo Ferroni Foundation
Via della Lastruccia 3 50019 Sesto Fiorentino (Italy)

Supporting Information and the ORCID identification number(s) for the author(s) of this article can be found under: http://dx.doi.org/10.1002/cphc.201601267.

water to these organic solutions results in the formation of reversed lamellar phases.[11]

We also synthesized similar derivatives from D-isoascorbic acid through the same reaction, and studied the effect of chirality of the polar head group in their phase behavior and self-assembly properties.[28,29]

Our aim in this work is twofold: 1) we report on the physicochemical characterization of new double-chained surfactants, namely, dialkanoyl-5,6-*O*-ascorbic acid esters (Di-ASC*n*; $n=8$, 10, or 12; see Figure 1), performed through differential scanning calorimetry (DSC), FTIR spectroscopy, and small- and wide-angle X-ray scattering (SAXS/WAXS) measurements; and 2) we discuss the relevance of the hydroxyl group in position 5 of the ascorbic acid ring in determining the hydration properties of these surfactants.

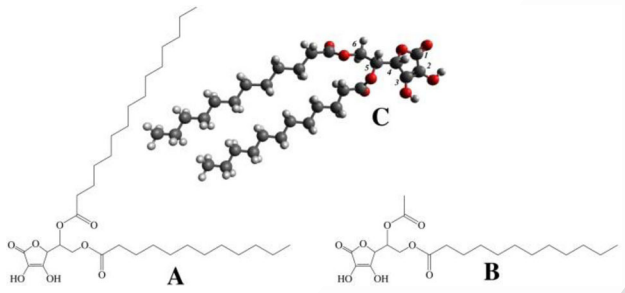

Figure 1. Structures of Di-ASC12 (A) and Ac-ASC12 (B). C) Minimized structure of Di-ASC12 and atom numbering for the ascorbic acid ring. Gray, red, and white spheres represent carbon, oxygen, and hydrogen atoms, respectively.

For the latter, we also investigated the properties of 5-acetyl-6-*O*-dodecanoyl L-ascorbic acid (Ac-ASC12), in which the hydroxyl group in position 5 was replaced by a short acetyl moiety. Our results show that functionalization of this —OH group results in a dramatic loss of polarity and hydration of the hydrophilic head, and in a significant reduction of the intermolecular HB capability.

2. Results and Discussion

The packing parameter, *p*, for a given amphiphile is calculated from Equation (1):

$$p = v/(lA_p) \quad (1)$$

in which *v*, *l* and A_p are the volume and length of the hydrocarbon chains and the area per polar head group, respectively. The value of *p*, which depends only on the geometric features of the amphiphile, can be used to predict the shape of the self-assembled structure produced in a suitable solvent.[30] The values of *v* and *l* are calculated according to the Tanford formulae [Eqs. (2) and (3)]:[31]

$$v = 27.4 + 26.9(n-1) \quad (2)$$

$$l = 1.5 + 1.265(n-1) \quad (3)$$

in which *n* represents the number of carbon atoms in the chain. The *p* values for Di-ASC*n* are all close to one; this indicates that these amphiphiles tend to form planar bilayers.

For all Di-ASC*n*, A_p was taken as 45 Å^2. The previously determined cross-section areas for single-chained L-ASC*n* esters range from 42 to 49 Å^2, as obtained by surface tensiometry or XRD analysis.[28] In the present case, we argue that the presence of a second alkyl tail in position 5 reduces further the polar head group area for two reasons: 1) the conversion of the free —OH into an ester group in position 5 produces reduced polarity and weaker hydration, and a lower intermolecular HB capability, resulting in a smaller A_p; and 2) by comparing L-ASC*n* and their D- counterparts, we observed in previous studies that A_p was always smaller in the D-isoascorbic monoalkyl esters than that in the L-ascorbic analogues with the same chain length because the former possessed more intramolecular HB, whereas the latter establish more intermolecular HB.[28]

The redox and acidic properties of L-ascorbic acid and its derivatives appear to be related to the furan ring, enediol group, and to the carbonyl in position 1. On the other hand, the biological effects of these molecules are mainly related to the side chain.[28,32,33] More particularly, the remarkably different biological activity of L-ascorbic and D-isoascorbic acid reflects their different hydration properties and different perturbation they induce in the dynamic structure of neighboring bulk water.[29,34–37]

All Di-ASC*n*, in particular, one-armed Ac-ASC12, show negligible solubility in water because the second aliphatic tail increases their hydrophobic character. Additionally, esterification of the secondary hydroxyl group in position 5 removes the hydration capability of the free —OH moiety, and thus, alters the set of hydrogen bonds established by the head group with the surrounding environment.

All derivatives are soluble in chloroform and acetone, whereas the solubility in cyclohexane depends on the chain length: Di-ASC8 is completely soluble up to 5 wt%, Di-ASC10 forms stable turbid suspensions, and Di-ASC12 produces viscous opaque samples.

The samples were investigated through DSC and SAXS to assess their physicochemical properties, thermal behavior, and structural features.

2.1. Characterization of the Pure Solids

2.1.1. DSC

The thermograms recorded for pure Di-ASC8, Di-ASC10, Di-ASC12, and Ac-ASC12 are reported in Figure 2. The temperature (T_{mp}), enthalpy■■ok?■■ (ΔH_{fus}), and entropy ($\Delta S_{fus} = \Delta H_{fus}/T_{mp}$) of melting of the double-chained derivatives are listed in Table S1 in the Supporting Information, together with those of the corresponding alkanes, alkanols, alkanoic acids, ethyl alkanoates, single-chain ascorbyl esters (L and D), and for the bola derivatives (LL, DD, and DL) we reported previously.■■refs.?■■

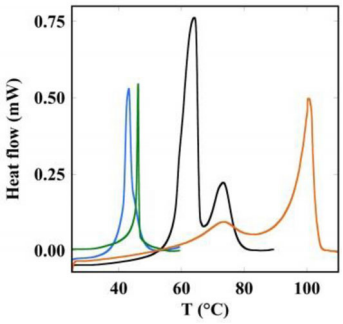

Figure 2. DSC scans of Di-ASC8 (black), Di-ASC10 (blue), Di-ASC12 (green), and Ac-ASC12 (red). Endo up.

Upon heating, Di-ASC8 and Di-ASC10 produce two partly overlapped endothermic peaks centered at 64.5 and 73.9 °C for the former and at 45.2 and 47.0 °C for the latter. The two peaks correspond to the melting of two polymorphs (a and b) that coexist in the solids. The same phenomenon is also found in the case of one-armed Ac-ASC12, with two peaks at 73.0 and 100.6 °C. We return to this observation later when we discuss the SAXS and FTIR spectroscopy results.

Instead, in the case of Di-ASC12 only one endothermic melting peak appears at about 46.2 °C.

The behavior of the single-chained surfactants is very different from that of their double-chained counterparts. For the former, the melting temperature and enthalpy change regularly increase with the chain length, as expected. On the other hand, for double-chained Di-ASC*n*, the melting temperature decreases upon increasing the length of the alkyl chain from 8 to 10 and then it remains approximately constant.

The entropy of fusion shows the highest value for alkanes at constant *n*; this reflects the high degree of disorder of the liquid state with respect to that in the solid phase. In the case of the alkanols, alkanoic acids, and esters, we recorded more complex behavior related to the effect of different head groups and their capability to establish HB.

Figure 3 shows the variation of ΔS_{fus} as a function of the alkyl tail length and illustrates that, for the alkanes, alkanols, alkanoic acids, and L- and D-ASC derivatives, the entropy change

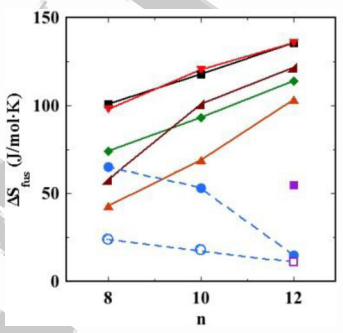

Figure 3. Entropy change of fusion (ΔS_{fus}, in J mol^{-1} K^{-1}) for alkanes (■), alkanols (▼), fatty acids (◆), L-ASCn (▲), D-ASC*n* (◢), Di-ASC*n* (● and ○) as a function of the number of carbon atoms in the alkyl chain, and for Ac-ASC12 (■ and □).

of melting increases more or less regularly with the number of carbon atoms in the chain.

This is generally ascribed to the effect of the longer alkyl chain and to the different set of HB interactions present in the crystals of L-ASC*n*, D-ASC*n*, alkanoic acids, and alkanols. The opposite trend is found for the double-chained derivatives Di-ASC*n*. Such an effect is probably due to weaker interactions that are established between the head groups in the solid state and to the particular arrangement of aliphatic chains in the crystalline structure, as discussed later.

2.1.2. SAXS

SAXS profiles reveal the presence of lamellar phases (Figure 4). For Di-ASC8 (black in Figure 4), the two diffraction peaks are not related to a single lamellar lattice, but show the presence of two coexisting phases with characteristic spacings of 16.6 and 27.3 Å. The SAXS profile for Di-ASC10 (red in Figure 4) shows the presence of a well-defined structure with a dimension of 17.4 Å.

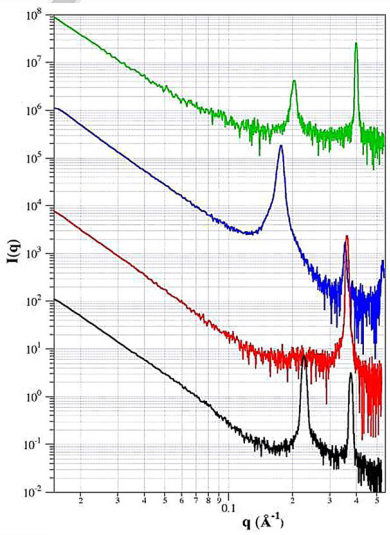

Figure 4. SAXS profiles of Di-ASC8 (black), Di-ASC10 (red), Di-ASC12 (blue) and Ac-ASC12 (green).

Moreover, we observe a very broad feature at about 0.2 Å^{-1}, presumably related to a second phase, the melting of which is observed in the DSC scans. The three peaks that appear in the case of Di-ASC12 (blue in Figure 4) are in full agreement with a single lamellar phase with a dimension of 35.7 Å. Finally, Ac-ASC12 (green in Figure 4) shows two diffraction peaks that could reflect the presence of a single lamellar phase with a spacing of 30.6 Å. However, both the remarkable intensity and narrowing of the second peak suggest the coexistence of a second lamellar phase with a dimension of 15.7 Å. Table 1■■ok? changed from Table 2■■ lists the spacings obtained from the SAXS experiments for the investigated specimens.

In the case of the single-chained derivatives, the spacing of the lamellar structure was found to be 31.4, 34.5, and 38.7 Å

Table 1. Length of the alkyl chain in its fully stretched conformation [*l*, in Å, see Eq. (3)], spacings (τ, in Å), and tilting angles (ψ) for the two crystalline structures 1 and 2 depicted in Figure 5.

	l [Å]	τ_1 [Å]	ψ_1 [°]	τ_2 [Å]	ψ_2 [°]
Di-ASC8	10.3	16.6	33	27.3	43
Di-ASC10	12.9	17.4	32	31.4	43
Di-ASC12	15.4	–	–	35.7	44
Ac-ASC12	15.4	15.7	26	30.6	37

for ASC8, ASC10, and ASC12, respectively. A comparison with the spacings found for double-chained Di-ASC*n* indicates that the presence of the second hydrocarbon chain brings about a significant contraction of the lamellar thickness. Such structural modification is due to stronger interchain van der Waals interactions, which keep the hydrocarbon tails closer and in a more compact arrangement. Furthermore, functionalization of the –OH group in position 5 reduces the hydration capability of the polar head, which presumably leads to an additional lowering of the lamellar thickness. The spacing of one-armed Ac-ASC12 is further reduced.

2.1.3. WAXS, FTIR, and Polymorphs

The spacings obtained from the SAXS data analysis suggest the presence of crystalline structures with different degrees of interdigitation and/or tilting of the molecules.

Figure 5 illustrates the two different forms in which the Di-ASC*n* molecules are tilted with (1) or without (2) interdigitation of the aliphatic chains. For different spacings, we calculated the two tilting angles (ψ_1 and ψ_2) by using Equation (4):

$$\tau = (2h + \alpha l)\sin\psi \qquad (4)$$

in which *h* is the length of the hydrophilic head group (10 Å) and α is the extent of interdigitation, that is, $\alpha = 1$ for fully interdigitated tails and $\alpha = 2$ for no interdigitation. The values of the tilting angles determined by Equation (4) and the lamellar thicknesses obtained by SAXS are reported in Table 1.

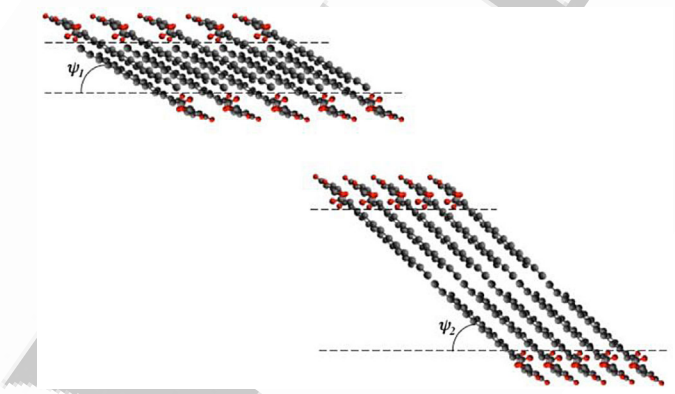

Figure 5. Phases formed in the solid state by Di-ASC*n*. Gray circles represent carbon atoms and red circles represent oxygen atoms. Hydrogen atoms are omitted for clarity. 1) Complete interdigitation of the alkyl chains; 2) no interdigitation of the hydrophobic chains. ψ_1 and ψ_2 are the tilting angles.

Polymorphism is a typical feature of fatty acids[38] and consists of the ability of a molecule to take more than one crystalline form, depending on its arrangement within the crystal lattice.[39]

Each polymorphic form is characterized by a distinct short spacing and the chain-length structure produces a repetitive sequence of acyl chains involved in a unit cell lamella along the long-chain axis.[38]

The polymorphic forms can be identified by means of WAXS and FTIR techniques.[40,41] Figures S1 and S2 in the Supporting Information show the WAXS profiles and FTIR spectra for the investigated samples in the solid state.

Long-chain alkanes and other organic molecules can form different crystalline phases: hexagonal (α_H), orthorhombic (β_O), triclinic (β_T), and monoclinic (β_M); these produce specific bands between 750 and 710 cm^{-1} in the FTIR spectra.[42]

Table 2 reports the characteristic experimental features that usually indicate the presence of a polymorph.

Table 2. FTIR and WAXS features for the detection of polymorphs.

Form	FTIR[28,42,43]	WAXS[28,42,43]	
	[cm^{-1}]	*d* [Å]	2θ [°]
α_H	720	4.2	21.5
β_O	719, 727	3.8, 4.2	21.5, 23.9
β_T	717	3.6, 3.8, 4.5	19.5, 22.5, 23.9

According to our results, Di-ASC8, Di-ASC10, and one-armed Ac-ASC12 show the presence of both β_O and β_T polymorphs, whereas only the β_O form is found for Di-ASC12.

2.2. Characterization of the Organogels

2.2.1. DSC

Upon heated, the organogel turns into a clear solution; therefore, the phase transition corresponds to collapse of the gel network. Figure S3 in the Supporting Information shows the thermogram for 15 wt% Di-ASC12/cyclohexane organogel, with a temperature peak at 26.7 °C and a transition enthalpy change of 26.1 $J g^{-}$.

2.2.2. SAXS

SAXS experiments were performed on Di-ASC12/cyclohexane dispersions at different surfactant contents: 0.25, 2, 5, and 15 wt% at 15 °C (see Figures 6 and 7). In another set of experiments, the 5 and 15% samples were first heated to 35 °C and then cooled back to 15 °C, to investigate the reversibility of the phase transition (see Figure S5 in the Supporting Information).

Figure 6 shows the SAXS profile obtained on the 0.25, 2, 5, and 15 wt% specimens at 15 °C.

Figure S4 in the Supporting Information shows the SAXS profiles for 5 and 15 wt% DiASC12/cyclohexane organogels,

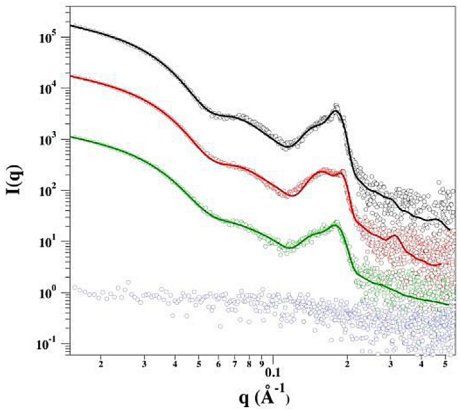

Figure 6. SAXS profiles for 0.25, 2, 5, and 15 wt% Di-ASC12/cyclohexane dispersions at 15 °C.

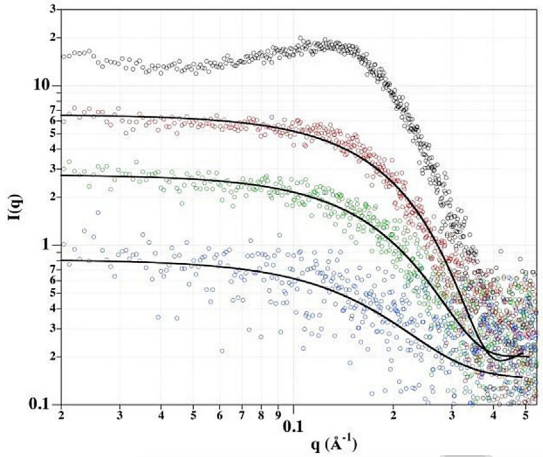

Figure 7. SAXS profiles for 0.25 wt% Di-ASC12 dispersion at 15 °C (blue), and 2 (green), 5 (red) and 10 wt% dispersions at 35 °C.

before and after the heating–cooling cycle. The plots indicate full reversibility of the phase transition that, according to the DSC data, occurs at around 27 °C.

The SAXS data acquired on samples in the gel state were fitted by a main contribution from the gel structure, that is, the "stacked discs" model (see the Supporting Information), combined with two extra terms related to the excess lamellar solid present in the sample.

The SAXS advanced model we adopted in this study allowed details of the nanostructure of the molecular assembly responsible for the rheological properties of the gel state to be determined. The piled arrangement of disc-like objects is reminiscent of the original lamellar structure of the solid phase, and depends on the sample concentration and temperature. Increasing the temperature of the system results in a reversible transition from stacked discs to reverse micelles.

The stacked-disc arrangement was obtained again after cooling, although the peak associated with the nondispersed solid was less evident. Structural fitting parameters extracted from the curves shown in Figure 6 and Figure S4 in the Supporting Information (according to the model depicted in the Supporting Information) are reported in Table 3.

Table 3. Structural parameters obtained from the SAXS profiles for the investigated organogel samples shown in Figure 6 and Figure S4 in the Supporting Information (see the Supporting Information for definitions).

	2%	5%	5% cool	15%	15% cool
R	65	66	75	68	76
2 h	18	16	18	18	18
d	11	12	9	11	9
n	3.7	3.6	2.5	3.6	2.4
*q*0	0.18	0.19	0.16	0.18	0.17
pow	−2.1	−2.2	−2.2	−2.3	−2.2

Fitting indicates that the gels are made up of building blocks that comprise approximately three stacked discs. In turn, these consist of lamellae with a hydrophilic core of 18 Å and a hydrophobic layer of about 10 Å. These dimensions are compatible with the calculated length of the head group (10 Å) and the length of the hydrophobic tail calculated according to Equation (3) (15.4 Å).

The disc radius is about 7 nm. The structure of the discs agrees with the assembly depicted by John et al.[44]

A comparison between the third and fourth columns and between the last two columns in Table 3 indicates that the gel state is recovered after cooling.■■ok?■■ The size differences before and after the heating–cooling treatment are within that of the resolution of the equipment. However, the piled up blocks become slightly larger and thinner after cooling with respect to the same structures in the original gels (see the values of *R* and *n* in Table 3).

The position of the peak due to the presence of nondispersed solid in the dispersion is the same as that previously determined for pure Di-ASC12 (i.e., $q = 0.18$ Å^{-1}). The Porod exponent (pow) is compatible with a 2D (lamellar) structure of the solid.

The SAXS curves obtained for the dilute sample (0.25 wt%) at 15 °C, and for higher Di-ASC12 contents at 35 °C are reported in Figure 7.

Data analysis was performed by adopting a model (see the Supporting Information) that described the scattering objects as spherical particles with a mean radius of about 10 Å. This finding agrees with the presence of reverse micelles with the hydrophilic core made up of polar head groups, whereas the aliphatic tails are extended in the dispersing phase. This arrangement brings about a negligible contrast between the hydrocarbon chains and solvent molecules, so that only the polar head region (micellar core) is responsible for scattering.

The mean radius of the inverse micelles and polydispersity are reported in Table 4.

At a surfactant content of 0.25 wt%, spherical aggregates are formed in solution at low temperature. This sample does not form a gel upon cooling. For more concentrated samples, the low-temperature organogel turns into micellar particles upon heating.

Moreover, we note that the SAXS curve for the most concentrated sample (15%) cannot be fitted by considering only the

Table 4. Structural parameters describing inverse micelles obtained in very diluted samples (0.25 %) at 15 °C and in concentrated samples (2 and 5 %) at 35 °C (see Figure 7).

	0.25 %	2 %	5 %
R_{avg}	7	10	10
polydispersity	0.37	0.15	0.08

spherical form factor due to the onset of an intermicellar interaction, as shown by the very broad peak at about 0.135 Å^{-1}. This behavior is similar to that previously found for a double-chained mono-substituted ascorbyl derivative (8ASC10).[11] The complete modeling of these curves is out of the scope of this paper.

3. Conclusions

Vitamin C based surfactants with two saturated alkyl chains with 8, 10, or 12 carbon atoms in positions 5 and 6 of the L-ascorbic acid ring (Di-ASC*n*) were synthesized and investigated. Their water solubility was very poor, although they were able to dissolve and aggregate in organic solvents. Similar to other ascorbyl derivatives, Di-ASC12 formed organogels in cyclohexane that turned into a micellar dispersion upon heating.

The most significant result of this study, however, was the observation that the –OH group in position 5 of ascorbic acid had a key role in imparting water solubility to ascorbyl amphiphiles. In the single-chain ASC*n* surfactants, the hydroxyl group in position 5 was free and could establish intermolecular hydrogen bonds that determined the stability and thermal of the self-assembled nanostructures. Therefore, the functionalization of the C5–OH group with another fatty acid chain in Di-ASC*n* not only increased the hydrophobic character of the entire surfactant, but it dramatically reduced its hydration and the possibility of interacting with other molecules through HB. Because the side chain in L-ascorbic and D-isoascorbic acids is usually considered the major■■incomplete sentence, please check■■

Experimental Section

Synthesis and Sample Preparation

All reactions were performed under an inert atmosphere of N_2. All chemicals were used as received without further purification. (*R*)-3,4-Bis(benzyloxy)-5-[(*S*)-1,2-dihydroxyethyl]furan-2(5*H*)-one was prepared according to a procedure reported in the literature (see the Supporting Information).[45,46] Flash column chromatography purifications were performed with silica gel 60 (230–400 mesh). TLC was performed with TLC plates coated with silica 376 gel 60 F254. NMR spectra were recorded in $CDCl_3$ on Varian Gemini 200 and Mercury 400 spectrometers operating at 200 and 400 MHz for ^{1}H, and 50 and 100 MHz for ^{13}C.

SAXS and WAXS

SAXS measurements were performed with a HECUS S3-MICRO camera (Kratky-type) equipped with two position-sensitive detectors (OED 50 M) containing 1024 channels of 54 μm in width. Cu Kα radiation ($\lambda = 1.542$ Å) was provided by an ultrabrilliant point microfocus X-ray source (GENIX-Fox 3D, Xenocs, Grenoble), operating at a maximum power of 50 W. The sample-to-detector distance was 281 mm. The volume between the sample and detector was kept under vacuum during the measurements to minimize scattering from the air. The Kratky camera was calibrated in the small-angle region by using silver behenate (58.34 Å),[47] whereas lupolen (4.12 and 3.8 Å) was used as a reference for the wide-angle region. SAXS curves were obtained in the scattering vector (q) range between 0.01 and 0.54 Å^{-1}, in which $q = (4\pi/\lambda)\sin\vartheta$; 2ϑ is the scattering angle. The WAXS region covered in the experiment was from 1.3 to 1.9 Å^{-1}. Samples were filled into 1.5 mm glass capillaries. Solid samples were investigated at 25 °C, whereas gel samples were analyzed both below and above the transition temperature. For the latter, the temperature was set to 15 and 35 °C, respectively, and controlled by a Peltier element, with an accuracy of ±0.1 °C. All scattering curves were corrected for the empty-cell contribution by considering the relative transmission factor.

DSC

Calorimetric measurements were performed on a Q1000 differential scanning calorimeter (TA Instruments). Samples were prepared by using hermetic aluminum pans sealed under a nitrogen atmosphere. The phase-transition temperature, T, was taken as the temperature of the endothermic peak, both for solid melting and for gel transition. The enthalpic change, ΔH, was determined by integrating the heat flow curve. All runs were performed at a rate of 2 °C min^{-1}.

FTIR spectroscopy

FTIR experiments were performed by using a Nexus 970-FTIR spectrometer (Thermo-Nicolet) with a KBr beam splitter and MCT/A detector. The instrument was equipped with an attenuated total reflectance (ATR) crystal, with a measuring bridge and a stamp to press the sample on the diamond. The energy range investigated was between $\tilde{\nu} = 4000$ and 650 cm^{-1}. The spectra were recorded with a resolution of 8 cm^{-1} and coadding 64 scans. All spectra were background corrected.

Reducing Activity

The reducing activity (RA, %) was evaluated by measuring the absorbance at $\lambda = 517$ nm of a solution of α,α-diphenylpicrylhydrazyl ■■ok?■■ (DPPH) in ethanol (10^{-4} M) before (A_0) and after 20 min (A_{20}) from the addition of an equal volume of the sample (10^{-4} M) in ethanol. RA is defined by Equation (5):

$$RA(\%) = 100(A_0 - A_{20})/A_0 \quad (5)$$

All derivatives possess a RA value larger than 95 %, comparable to those of L-ascorbic acid and its derivatives.[2]

Acknowledgements

We acknowledge CSGI for partial financial support and the Enzo Ferroni Foundation for helpful discussions.

Conflict of interest

The authors declare no conflict of interest.

Keywords: amphiphiles · gels · hydrogen bonds · polymorphism · surfactants

[1] E. Carretti, V. Mazzini, E. Fratini, M. Ambrosi, L. Dei, P. Baglioni, P. Lo Nostro, *Phys. Chem. Chem. Phys.* **2016**, *18*, 8865 – 8873.
[2] P. Lo Nostro, G. Capuzzi, A. Romani, N. Mulinacci, *Langmuir* **2000**, *16*, 1744 – 1750.
[3] G. Capuzzi, P. Lo Nostro, K. Kulkarni, J. E. Fernandez, *Langmuir* **1996**, *12*, 3957 – 3963.
[4] G. Capuzzi, P. Lo Nostro, K. Kulkarni, J. E. Fernandez, F. F. Vincieri, *Langmuir* **1996**, *12*, 5413 – 5418.
[5] G. Capuzzi, K. Kulkarni, J. E. Fernandez, F. F. Vincieri, P. Lo Nostro, *J. Colloid Interface Sci.* **1997**, *186*, 271 – 279.
[6] S. Palma, P. Lo Nostro, R. H. Manzo, D. Allemandi, *Eur. J. Pharm. Sci.* **2002**, *16*, 37 – 43.
[7] S. Palma, R. H. Manzo, D. Allemandi, L. Fratoni, P. Lo Nostro, *J. Pharm. Sci.* **2002**, *91*, 1810 – 1816.
[8] C. Venturini, C. Pomposi, E. Carretti, E. Fratini, P. Lo Nostro, P. Baglioni, *J. Phys. Chem. B* **2014**, *118*, 3053 – 3062.
[9] M. Ambrosi, E. Fratini, V. Alfredsson, B. W. Ninham, R. Giorgi, P. Lo Nostro, P. Baglioni, *J. Am. Chem. Soc.* **2006**, *128*, 7209 – 7214.
[10] C. Dolle, P. Magrone, S. Riva, M. Ambrosi, E. Fratini, N. Peruzzi, P. Lo Nostro, *J. Phys. Chem. B* **2011**, *115*, 11638 – 11649.
[11] P. Lo Nostro, R. Ramsch, E. Fratini, M. Lagi, F. Ridi, E. Carretti, M. Ambrosi, B. W. Ninham, P. Baglioni, *J. Phys. Chem. B* **2007**, *111*, 11714 – 11721.
[12] P. Lo Nostro, G. Capuzzi, P. Pinelli, N. Mulinacci, A. Romani, F. F. Vincieri, *Colloids Surf. A* **2000**, *167*, 83 – 93.
[13] S. Palma, R. H. Manzo, D. Allemandi, L. Fratoni, P. Lo Nostro, *Langmuir* **2002**, *18*, 9219 – 9224.
[14] P. Lo Nostro, B. W. Ninham, L. Fratoni, S. Palma, R. H. Manzo, D. Allemandi, P. Baglioni, *Langmuir* **2003**, *19*, 3222 – 3228.
[15] P. Lo Nostro, B. W. Ninham, M. Ambrosi, L. Fratoni, S. Palma, D. Allemandi, P. Baglioni, *Langmuir* **2003**, *19*, 9583 – 9591.
[16] S. Palma, R. H. Manzo, P. Lo Nostro, D. Allemandi, *Int. J. Pharm.* **2007**, *345*, 26 – 34.
[17] S. Borsacchi, M. Ambrosi, P. Lo Nostro, M. Geppi, *J. Phys. Chem. B* **2010**, *114*, 15872 – 15878.
[18] M. Ambrosi, P. Lo Nostro, L. Fratoni, L. Dei, B. W. Ninham, S. Palma, R. H. Manzo, D. Allemandi, P. Baglioni, *Phys. Chem. Chem. Phys.* **2004**, *6*, 1401 – 1407.
[19] A. Muga, H. L. Casal, *J. Phys. Chem.* **1990**, *94*, 7265 – 7271.
[20] M. Kodama, S. Seki, *Adv. Colloid Interface Sci.* **1991**, *35*, 1 – 30.
[21] M. Tsuchiya, K. Tsujii, K. Maki, T. Tanaka, *J. Phys. Chem.* **1994**, *98*, 6187 – 6194.
[22] J. M. Vincent, A. Skoulios, *Acta Crystallogr.* **1966**, *20*, 432 – 440.
[23] H. Sapper, D. G. Cameron, H. H. Mantsch, *Can. J. Chem.* **1981**, *59*, 2543 – 2549.
[24] U. Köhler, P. W. Yang, S. Weng, H. H. Mantsch, *Can. J. Spectr.* **1988**, *33*, 122 – 127.
[25] S. Nandi, H.-J. Altenbach, B. Jakob, K. Lange, R. Ihizane, M. P. Schneider, *Org. Lett.* **2011**, *13*, 1980 – 1983.
[26] D. Dasgupta, S. Srinivasan, C. Rochas, A. Ajayaghosh, J.-M. Guenet, *Soft Matter* **2011**, *7*, 9311 – 9315.
[27] S. S. Babu, V. K. Praveen, A. Ajayaghosh, *Chem. Rev.* **2014**, *114*, 1973 – 2129.
[28] M. Ambrosi, P. Lo Nostro, E. Fratini, L. Giustini, B. W. Ninham, P. Baglioni, *J. Phys. Chem. B* **2009**, *113*, 1404 – 1412.
[29] P. Lo Nostro, M. Ambrosi, B. W. Ninham, P. Baglioni, *J. Phys. Chem. B* **2009**, *113*, 8324 – 8331.
[30] J. N. Israelachvili, D. J. Mitchell, B. W. Ninham, *J. Chem. Soc. Faraday Trans. 2* **1976**, *72*, 1525 – 1568.
[31] C. Tanford, *J. Phys. Chem.* **1972**, *76*, 3020 – 3024.
[32] J. C. Leffingwell, *Chirality & Bioactivity 1, Pharmacology*, Leffingwell Reports, Canton, GA, **2003**, pp. 8 – 10.
[33] J. Hvoslef, *Acta Crystallogr. Sect. B* **1969**, *25*, 2214 – 2223.
[34] Y. Wang, Y. Tominaga, *J. Chem. Phys.* **1996**, *104*, 1 – 6.
[35] T. Umehara, Y. Tominaga, A. Hikida, S. Mashimo, *J. Chem. Phys.* **1995**, *102*, 9474 – 9479.
[36] S. Mashimo, N. Miura, T. Umehara, *J. Chem. Phys.* **1992**, *97*, 6759 – 6765.
[37] Y. Wang, Y. Tominaga, *J. Phys. Soc. Jpn.* **1993**, *62*, 4198 – 4201.
[38] K. Sato, *Chem. Eng. Sci.* **2001**, *56*, 2255 – 2265.
[39] K. Larsson, *Acta Chem. Scand.* **1966**, *20*, 2255 – 2260.
[40] S. T. Hyde in *Handbook of Applied Surface and Colloid Chemistry* (Eds.: K. Holmberg, D. O. Shah, M. J. Schwuger), Wiley, Chichester, **2001**, pp. 299 – 332.
[41] J. Yano, K. Sato, F. Kaneko, D. M. Small, D. R. Kodali, *J. Lipid Res.* **1999**, *40*, 140 – 151.
[42] B. Ren, Z. Cheng, Z. Tong, X. Liu, C. Wang, F. Zeng, *Macromolecules* **2006**, *39*, 6552 – 6557.
[43] M. Iwahashi, S. Takebayashi, M. Taguchi, Y. Kasahara, H. Minami, H. Matsuzawa, *Chem. Phys. Lipids* **2005**, *133*, 113 – 124.
[44] P. K. Vemula, U. Aslam, V. A. Mallia, G. John, *Chem. Mater.* **2007**, *19*, 138 – 140.
[45] H.-I. Choi, H.-J. Kim, J.-I. Park, E.-H. Shin, D.-W. Kim, S.-S. Kim, *Bioorg. Med. Chem. Lett.* **2009**, *19*, 2079 – 2082.
[46] D. Tanini, M. Gori, F. Bicocchi, M. Ambrosi, P. Lo Nostro, A. Capperucci, *Arkivoc* **2017**, *part ii*, 407 – 420.
[47] T. N. Blanton, M. Rajeswaran, P. W. Stephens, D. R. Whitcomb, S. T. Misture, J. A. Kaduk, *Powder Diffr.* **2011**, *26*, 313 – 320.

Manuscript received: November 17, 2016
Accepted Article published: March 20, 2017
Final Article published: ■■ ■■, 0000

*E. Tempestini, M. Bucci, V. Mastromartino, M. Gori, D. Tanini, M. Ambrosi, E. Fratini, A. Capperucci, P. Lo Nostro**

■■ – ■■

Organogels from Double-Chained Vitamin C Amphiphilic Derivatives

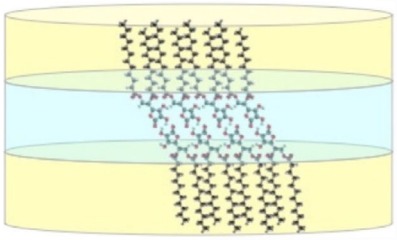

Surfactant stacks: Lamellar discs are observed in organogels obtained from double-chained vitamin C surfactants. The figure depicts the sequence of hydrophobic (yellow) and hydrophilic (blue) layers, as determined by small-angle X-ray scattering analysis.

Structures of #surfactants derived from vitamin C form #organogels @UNI FIRENZE SPACE RESERVED FOR IMAGE AND LINK

Share your work on social media! *ChemPhysChem* has added Twitter as a means to promote your article. Twitter is an online microblogging service that enables its users to send and read text-based messages of up to 140 characters, known as "tweets". Please check the pre-written tweet in the galley proofs for accuracy. Should you or your institute have a Twitter account, please let us know the appropriate username (i.e., @accountname), and we will do our best to include this information in the tweet. This tweet will be posted to the journal's Twitter account @ChemPhysChem (follow us!) upon online publication of your article, and we recommended you to repost ("retweet") it to alert other researchers about your publication.

Please check that the ORCID identifiers listed below are correct. We encourage all authors to provide an ORCID identifier for each coauthor. ORCID is a registry that provides researchers with a unique digital identifier. Some funding agencies recommend or even require the inclusion of ORCID IDs in all published articles, and authors should consult their funding agency guidelines for details. Registration is easy and free; for further information, see http://orcid.org/.

Elia Tempestini
Martina Bucci
Vincenzo Mastromartino
Marianna Gori
Dr. Damiano Tanini
Dr. Moira Ambrosi
Dr. Emiliano Fratini
Dr. Antonella Capperucci
Prof. Pierandrea Lo Nostro http://orcid.org/0000-0003-4647-0369

Author Contributions

P.L. Conceptualization: Lead; Data curation: Supporting; Formal analysis: Lead; Investigation: Lead; Resources: Lead; Supervision: Lead; Validation: Lead; Writing – original draft: Lead; Writing – review & editing: LeadE.T. Data curation: Supporting; Writing – original draft: SupportingM.B. Data curation: Supporting; Writing – original draft: SupportingV.M. Data curation: Supporting; Writing – original draft: SupportingM.G. Data curation: Supporting; Writing – original draft: SupportingD.T. Conceptualization: Equal; Data curation: Equal; Writing – original draft: SupportingM.A. Conceptualization: Equal; Data curation: Lead; Formal analysis: Equal; Investigation: Equal; Validation: Equal; Writing – original draft: LeadE.F. Formal analysis: Lead; Investigation: Equal; Writing – original draft: EqualA.C. Data curation: Equal; Supervision: Equal; Writing – original draft: Supporting.

These are not the final page numbers!